frontiers | Frontiers in Earth Science

ORIGINAL RESEARCH
published: 20 June 2022
doi: 10.3389/feart.2022.895604

Genetic Analysis of Abnormally High Ground Temperature From the Existence of Magmatic Rock Beneath Pingdingshan Coalfield

*Qi Wang[1], Jiajia Liao[2], Dongxu Zhou[1], Quanlin Hou[3] and Xinyi Wang[2,4,5]**

[1]College of Geosciences and Engineering, North China University of Water Resources and Electric Power, Zhengzhou, China, [2]Institute of Resources & Environment, Henan Polytechnic University, Jiaozuo, China, [3]College of Earth Science, University of Chinese Academy of Sciences, Beijing, China, [4]Collaborative Innovation Center of Coalbed Methane and Shale Gas for Central Plains Economic Region, Jiaozuo, China, [5]Collaborative Innovation Center of Coal Work Safety and Clean High Efficiency Utilization, Jiaozuo, China

Studies on the genetic mechanisms of abnormally high ground temperatures in coalfields are of great significance for the efficient mining of coal mines and the development and utilization of geothermal water. Therefore, we measured the temperature of 45 Cambrian limestone groundwater samples, thermal conductivity values of 11 Cambrian limestone samples, and the contents of uranium, thorium, and potassium-40 of 40 rock samples, aiming to ascertain the heat source of the abnormally high ground temperature in the Pingdingshan coalfield. The results show that the average geothermal gradient in the coalfield is about 3.32°C/100 m, and the calculated values of the average ground heat flow are about 104.28 mW/m^2, which demonstrate the abnormally high ground temperature in Pingdingshan coalfield. We also concluded that the whole radiogenic heat generation in sedimentary and magmatic rocks is 1.53 mW/m^2, whose contribution rate to the local geothermal flow is only 1.47%. Hence, we can infer that magmatic rocks exposed in or near the coalfield area may supply the heat source for the abnormally high ground temperature beneath Pingdingshan coalfield. A comprehensive analysis further shows that the latest intrusion time of the magmatic rock mass in the coalfield was 35 Ma; its lava temperature was 900°C, its cooling rate is 20.0°C/Ma, and the calculated residual temperature is more than 200.0°C. These values support the idea that the magmatic rocks may be the primary cause of the abnormally high ground temperature in the Pingdingshan coalfield.

Keywords: terrestrial heat flux, radionuclide exothermic, magmatic heat generation, residual temperature, Pingdingshan mining area

Edited by:
Wenjing Lin,
Chinese Academy of Geological Sciences, China

Reviewed by:
Zhuting Wang,
China University of Mining and Technology, China
Fengxin Kang,
Shandong Provincial Bureau of Geology and Mineral Resources (SPBGMR), China

****Correspondence:***
Xinyi Wang
wangxy@hpu.edu.cn

Specialty section:
This article was submitted to Geochemistry, a section of the journal Frontiers in Earth Science

Received: *14 March 2022*
Accepted: *16 May 2022*
Published: *20 June 2022*

Citation:
Wang Q, Liao J, Zhou D, Hou Q and Wang X (2022) Genetic Analysis of Abnormally High Ground Temperature From the Existence of Magmatic Rock Beneath Pingdingshan Coalfield. Front. Earth Sci. 10:895604. doi: 10.3389/feart.2022.895604

1 INTRODUCTION

Monitoring data have shown that the average geothermal gradient of the Pingdingshan coalfield is 3.32°C/100 m. At a buried depth of 1,000 m, the temperature can reach as high as 49.57°C in the rocks or groundwater. Hence, it is an area with an abnormally high ground temperature compared to other zones in Henan Province. Affected by the higher surrounding rock temperature and roof-pouring (gushing) water, the ambient temperature and air humidity of the underground mining space are

very high so that it not only increases the cost of coal mining, but also affects the physical and mental health and labor efficiency of the workers. Therefore, in this study an analysis of the genetic mechanism responsible for the abnormally high coalfield ground temperature seems to be of great significance.

In recent years, many scholars have focused on researching the heat-source mechanism of different geothermal areas via studying the heat production of radioisotopes and magmatic rocks. Burns et al. (2015) studied the steep permeability drop and low heat flow anomaly of a middle plateau aquifer system on the Columbia Plateau, which contains a heat flow regime at depths of 600–900 m. Their research showed that the steep permeability drop is related to hydrothermal transformation and pore-refilling minerals in the volcanic area. Peng et al. (2015) studied the geothermal field in the Linhuan mining area of the Huaibei coalfield and concluded that the high geothermal gradient mainly occurs in areas containing intensively developed anticlines and faults, and a high-temperature anomaly also occurs mainly in areas with intensively developed folds, uplifts, and faults (Jun et al., 2015). Ren et al. (2017) calculated the heat generation rate of coal-measure sedimentary rocks and magmatic rocks based on the natural gamma (GR) logging values of 6,208 coal-measure rocks taken from 36 boreholes in the Zhuji coalfield, Huainan, China. Generally speaking, the contribution of radiogenic heat generation of coal-measure rocks to terrestrial heat flow in the area is small, but the high heat generation rate of magmatic rocks has changed the heat generation structure of the rock strata greatly. Hasterok et al. (2018) analyzed the radiogenic heat generation of 204,000 whole rock geochemical data. Their research showed that the radiogenic heat generation of igneous and metamorphic igneous rocks increases with an increase of SiO_2 and K_2O, and decreases with an increase of Fe_2O_3, MgO, and CaO; meanwhile, the heat production of sedimentary and metamorphic rocks increases with an increase of Al_2O_3, FeO, TiO_2, and K_2O, but decreases with an increase of CaO. According to 39,933 and 6,465 Precambrian rock samples collected in Sweden and Finland, Veikkolainen et al. (2019) measured the concentrations of radioactive uranium, thorium, and potassium and calculated the heat generation rate. Their calculations showed that the average radiogenic heat generation rate of Precambrian rock samples in Sweden and Finland is $2.4 \pm 1.6\ \mu W/m^3$ and $1.42 \pm 1.41\ \mu W/m^3$, respectively; hence, the heat-production rate in Sweden is much higher than that in Finland (Veikkolainen and Kukkonen, 2019). Scharfenberg et al. (2019) tested and performed calculations of a Bohemia block in Germany, showing that the radiogenic heat generation rate in the granite is 3.9–8.9 $\mu W/m^3$, with an average of 4.9 $\mu W/m^3$, implying a medium-to-high heat-generation rate. The contribution of radiogenic heat generation should be considered in simulations of geothermal genetic mechanism. Erbek and Dolmaz (2019) showed that the heat flow to the southeast of the Aegean Sea and western Turkey is 50–125 mW/m^2, while the radiogenic heat generation rate is 0.21–0.51 $\mu W/m^3$. They found that the high heat flow value is closely related to seismic and tectonic activity in this area. Wang et al. (2019) analyzed the thermal state and geothermal potential of the lithosphere in the Xiong'an New Area, and their results showed that the average heat flux in the study area is 70.5 mW/m^2, higher than that on the Chinese mainland, which is 61.5 mW/m^2, and the crustal temperature at a depth of 40 km is 750–1,100°C.

Zhao et al. (2020) studied the geothermal mechanism of the hot dry rock (HDR) area in the Gonghe Basin, and they found that magma chambers and molten granite in the upper crust may be important heat sources for the HDR in Gonghe Basin, and that heat is transmitted through the near formation fractures, making Gonghe Basin a potential geothermal area. Song et al. (2020) calculated the radiogenic heat generation rate of a magmatic rock mass in southeast Jiangxi. Their research showed that the heat generation rate increases as the age of the rock mass decreases, and the heat generation rate of the Yanshanian magmatic rocks shows an obvious law of high in the south, low in the north, high in the west, and low in the east (Lu-sheng et al., 2020). Zhang et al. (2020a) calculated the heat production of radioactive elements of granitoids in the Gonghe Basin and Qinghai Tibet Plateau, and found that the abnormal heat flow in the Gonghe Basin may be a result of the combined action of radioactive element radiation heat generation in the thick crust and local thermal anomalies. According to the research of Sun et al. (2020), the ground heat flow value in southeast Guangxi is between 80 and 100 mW/m^2, and the temperature gradient is higher than 30°C/km. They concluded that the higher radionuclide content in the Indosinian granite in the area is the basis of the stable heat source. Based on the radiogenic heat generation rate data of 98 rock samples collected from the Gonghe Basin, Zhang et al. (2020b) analyzed the distribution characteristics of the radiogenic heat generation rate of main lithologic rocks in the basin and established a genetic model of the HDR geothermal resources in the area. Luo et al. (2020) calculated 6,094 radiogenic heat generation rates in the sedimentary layers in the Tarim Basin, finding an average value of $1.17 \pm 0.336\ \mu W/m^3$. Mudstone has the highest heat generation rate, followed by sandstone, dolomite, and limestone, and lithology is the main factor affecting the heat generation rate. It was estimated that the heat flow contribution from radiogenic heat generation is 9.36 mW/m^2, accounting for about 21% of the total surface heat flow. The radiogenic heat generation also has an impact on the geothermal field in the Tarim Basin. Ogunsanwo et al. (2021) calculated the radiogenic heat production rate for 30 rock samples from 10 quarries in Ogun State, Nigeria, which showed a range of values of 0.549–3.122 $\mu W/m^3$, in which uranium contributes the most and thorium contributes the least. Weinert et al. (2021) calculated the radionuclide heat production rate based on 30 Triassic, Silurian, Ordovician, and Devonian intrusive rocks extracted from a complex in the Gonghe Basin. Their study showed that the heat production rate of radioactive elements in this area is less than 1 $\mu W/m^3$ in biotite granite, and greater than 5 $\mu W/m^3$ in syenogranite. Ma et al. (2021) found that the deep heat source of a geothermal abnormity in the eastern Himalayan structural junction area mainly comes from the Yarlung Zangbo River junction zone and nearby deep faults, and the surface heat is mainly controlled by secondary tension and torsion faults on both sides of the junction zone (Xin et al., 2021).

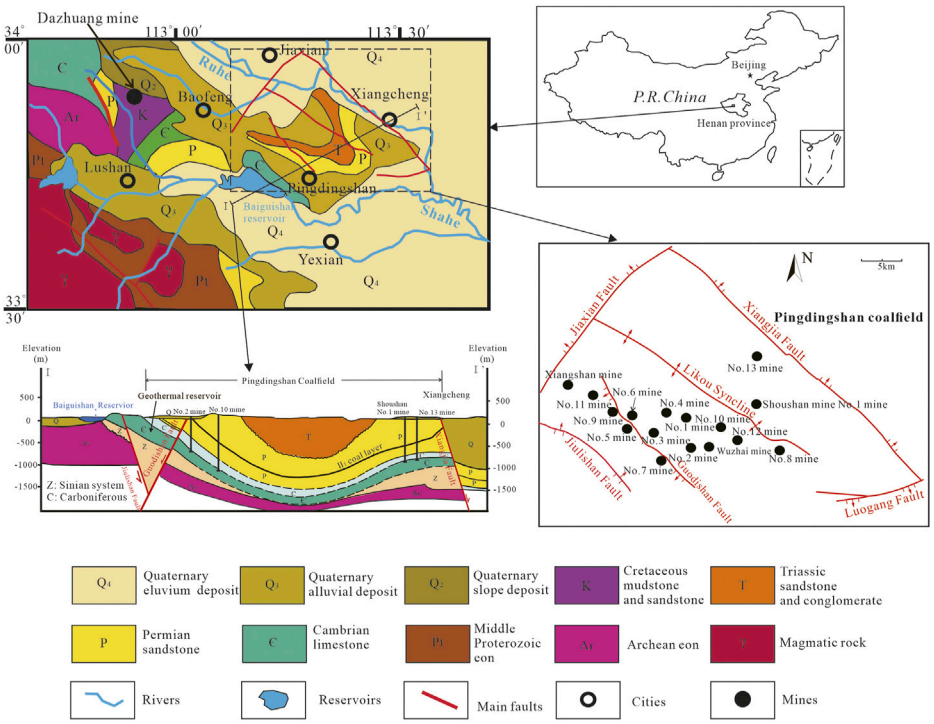

FIGURE 1 | Geological setting and mine positions in the Pingdingshan coalfield.

Regarding the abnormally high ground temperature in Pingdingshan coalfield, Zhang et al. (2000) analyzed the influence of groundwater migration on the temperature field based on the silica temperature scale method and isotope method, and expounded the causes of the uneven temperature distribution in the geothermal field. Based on an analysis of the distribution characteristics of the geothermal field in the Pingdingshan coalfield, Cao et al. (2014) clarified that the abnormal high-temperature area has the characteristics of a dense development of faults and fractures and fold uplift. The geothermal distribution is affected by the regional geological structure, groundwater activities, rock properties, and caprock properties (Bingqi et al., 2014).

Overall, studies on the abnormity of the ground temperature and its influencing factors in the Pingdingshan coalfield have been extensive, but there has been less research regarding the genetic mechanism of the abnormally high ground temperature. Therefore, based on field-measured data and geological setting conditions, we further studied the heat source of the abnormally high ground temperature in the Pingdingshan coalfield. The conclusions in this study may provide support for preventing and controlling mine heat damage, and promoting the development and utilization of geothermal water in the future.

2 GEOLOGICAL AND GEOTHERMAL CHARACTERISTICS

The Pingdingshan coalfield is located on an uplift fault block surrounded by the Jiaxian Fault, Xiangjia Fault and Luogang Fault, with an east–west length of 40 km and a north–south width of 10–20 km, and the mining area is about 650 km^2 (**Figure 1**). At present, Pingdingshan coalfield mainly mines the II_1 coal bed with a depth ranging from 680 to 1,000 m, which represents a deep mining state.

The strata of the Pingdingshan coalfield includes an Archean metamorphic rock series, Archaean, upper Proterozoic Sinian, lower Paleozoic Cambrian, upper Paleozoic Carboniferous and Permian, Mesozoic Triassic, Cenozoic Neogene and Quaternary (**Figure 1**). A histogram of the stratum lithology in Pingdingshan coalfield is shown in **Figure 2**. The geothermal reservoirs in the Pingdingshan abnormity area are thick limestone composed of an upper Cambrian Gushan Formation and middle Zhangxia Formation. For buried stratum depths less than 420 m, karst caves of different sizes and shapes are densely distributed and karst is relatively developed. For buried depths greater than 420 m, the distributions of karst layers are variable, and there are no karst caves. Generally, the karst is not as developed as in the upper part, but at the intersection of structural development zones and faults, karst pores, karst gaps, and fractures are relatively developed.

The main structure in the area is a wide and gentle compound Likou syncline with many secondary folds located to the south and north of the Likou syncline axis. There also exists some large and medium-sized faults in Pingdingshan coalfield, such as Guodishan Fault, and most of them are blocking faults. The simple geological setting of the Pingdingshan coalfield is shown in **Figure 1**.

Rock stratigraphic units				Thickness (m)	Lithological description
Erathem	System	Formation	Designator		
Cenozoic	Quaternary		Q	0~430	Gravel, pebbles and sand dominate.
	Neogene		N	0~200	The lower part is sandstone and the middle and upper part is sandy mudstone.
Mesozoic	Triassic	Ermaying	T_{2E}	0~250	Feldspathic quartz sandstone and feldspathic sandstone.
		Liujiagou	T_{1l}	0~250	Medium and fine-grained sandstone interspersed with calcareous siltstone.
Upper Paleozoic	Permian	Shiqianfeng	P_{22}	0~312	Sandstone and sandy mudstone.
		Upper-Shihezi	P_{21}	0~390	Sandstone, sandy mudstone and thin coal seams.
		Lower-Shihezi	P_{12}	0~397	Sandstone, sandy mudstone, mudstone and coal seams.
		Shanxi	P_{11}	84	Sandstone, sandy mudstone and coal seams.
	Carboniferous	Taiyuan	C_{3t}	30~80	Limestone, sandstone, sandy mudstone and coal seams.
		Benxi	C_{2b}	0~20	Limonite, oolitic aluminous mudstone and very unstable thin coal seams.
Lower Paleozoic	Cambrian	Fengshan	$\in_{3f}$	0~38	Cryptocrystalline dolomitic limestone, thinly bedded mudstone and grey dolomite.
		Changshan	$\in_{3ch}$	0~66	Dolomitic limestone, mudstone and dolomite.
		Gushan	$\in_{3g}$	25~32	Fine-grained dolomite and oolitic dolomite.
		Zhangxia	$\in_{2zh}$	60~220	Oolitic dolomite.
		Xuzhuang	$\in_{2x}$	50~250	Medium-thickly bedded muddy-striped limestone, dolomitic limestone.
		Maozhuang	$\in_{2m}$	90~140	Siltstone.
		Mantou	$\in_{13}$	220	Shale and limestone.
		Xinji	$\in_{11}$	55~210	Medium to coarse grained quartz sandstone, leopard skin limestone and dolomitic limestone.
Upper Proterozoic	Sinian	Luoquan	Z_{3l}	100	The lower part is an ice-covered sandy conglomerate and the upper part is a sandy mudstone.
		Luoyukou	Z_{3ly}	320	Thickly bedded siliceous streaked dolomite.
		Sanjiaotang	Z_{3s}	100	Thickly bedded medium to fine-grained quartz sandstone.
		Cuizhuang	Z_{3c}	290	Sandy shale.
		Beidajian	Z_{2bd}	241~280	Thickly bedded fine and medium grained quartz sandstone.
		Baicaoping	Z_{2b}	166~180	Muddy siltstone and sandy mudstone.
		Yunmengshan	Z_{2y}	177~533	Quartz sandstone.
		Majiahe	Z_{1m}	1,580~2,220	Metamorphic andesite.
Archaean		Zhaoanzhuang	A_{rz}	>2,950	Plagioclase gneisses and hornblende gneisses.

FIGURE 2 | Histogram of stratum lithology.

3 DATA AND METHODS

In order to ascertain the heat source of Pingdingshan geothermal abnormal area, a total of 45 temperature values were measured at the outlets of geothermal wells and drains in the Pingdingshan coalfield, and the locations, measured temperatures, and corresponding geothermal gradients are shown in **Table 1**.

In the Pingdingshan coalfield and neighboring Ruzhou coalfield, 11 limestone samples were collected from the Cambrian strata, and the values of the thermal conductivity were determined by Chinese Academy of Geological Sciences using thermal conductivity scanning (TCS), with a determining range of 0.20–25 W/(mK). The uncertainty of measured results was about 3%, and the results are shown in **Table 2**.

To obtain the radionuclide contents (uranium, thorium, and potassium-40) in the stratum of the Pingdingshan coalfield, 40 rock samples were collected from surface rock belts and geological drilling holes. At Beijing Research Institute of Uranium Geology (BRIUG), the contents of uranium and thorium were both measured by inductively coupled plasma mass spectrometry (ICP-MS; PerkinElmer Elan DCR-e), and the uncertainties were lower than 10% with a determining range of 0.05×10^{-6} to $1{,}000 \times 10^{-6}$ mg/kg. The content of potassium-40 was determined by atomic absorption spectroscopy (z-2000) with an uncertainty lower than 2%. The densities of the rock samples were measured with a densitometer (AKD-120A) with a measurement precision and uncertainty of 0.0001 g/cm^3 and 2%, respectively, in the laboratory of Henan Polytechnic University. All the measured values are shown in **Table 3**.

TABLE 1 | Geothermal gradient of cap rock in different mines.

Locations	Depth (m)	Well head temperature (°C)	Geothermal gradient (°C/100 m)
Special return air roadway of No. 2 mine	508	27	2.03
31,010 air roadway of No. 2 mine	790	41	3.11
Lower concentration roadway of No. 2 mine	818.7	40	2.87
Downhill drilling of geng-1 belt in No. 2 mine	916	41.5	2.73
Cambrian hydrological hole of No. 3 mine	690	42	3.73
Geng-1 Drainage hole of No. 4 mine	627	40	3.79
Downhill 18# hole of No.4 mine	902.5	43.5	3.00
G18 + 3 m drainage hole of No. 4 mine	1,017	43	2.60
Drainage hole in F19 of No. 4 mine	1,055	48	2.99
Shimen water inrush point of No. 5 mine	616	40	3.86
320 water inrush point of No. 5 mine	622	45	4.66
Ji-2 water bunker of No. 5 mine	975	46	3.03
The downhill in the geng-2 area of No. 7 mine	355	21.5	1.30
13,141 cut hole of No. 8 mine	465	36	4.27
Ji-3 return air roadway of No. 8 mine	513	37	4.06
11,032 drain hole of No. 8 mine	585	40.7	4.20
13,011 drain hole of No. 8 mine	598	40.7	4.10
13,022 drain hole of No. 8 mine	590	38	3.68
West roadway 1# hole of No. 8 mine	680	49	4.85
West roadway 2# hole of No. 8 mine	760	49	4.33
West roadway 3# hole of No. 8 mine	843	52	4.25
West roadway 4# hole of No. 8 mine	850	49	3.85
West roadway 5# hole of No. 8 mine	860	49	3.81
West roadway 6# hole of No. 8 mine	875	49	3.74
West roadway 7# hole of No. 8 mine	925	49	3.53
Ji-2 lower extension sump of No. 8 mine	1,179	47	2.58
-618 hydrological hole of No. 9 mine	893	37.5	2.34
Ji-4 water bunker of No. 10 mine	1,106.8	51	3.12
Hydrological hole of No. 11 mine	543	23	1.12
Hydrological hole 2 of No. 12 mine	1,091	54	3.45
5# drain hole of No. 12 mine	1,119	52	3.18
7# drain hole of No. 12 mine	1,114	54	3.38
Hydrological hole of No. 13 mine	580	45	5.01
Inrush point 1# of No. 13 mine	584	38	3.72
Inrush point 2# of No. 13 mine	660	27	1.54
Inrush point 3# of No. 13 mine	590	27	1.73
Inrush point 4# of No. 13 mine	627	42	4.12
Inrush point 5# of No. 13 mine	823	53	4.49
Ji-3 bunker mouth of No. 13 mine	822	49	3.99
Hydrological hole of Xiangshan mine	293	22	1.79
Hydrological hole of Wuzhai mine	438	26	2.13
2# hole in transportation roadway of Wuzhai mine	457.2	26	2.03
-7,604 hole of Shoushan No.1 mine	633	51	5.56
-769 sump of Shoushan No.1 mine	891.7	50	3.78
Civil well near to Jiaxian	421	25	1.97
Mean Value			3.32

4 RESULTS AND DISCUSSION

4.1 Characteristics of the Geothermal Gradient

The temperature of the constant-temperature zone in Pingdingshan is 17.2°C, and the depth of the constant temperature zone is about 25 m. According to the measured temperatures of the 45 groundwater samples of Cambrian limestone, the geothermal gradient of the Pingdingshan coalfield was calculated, and the calculated results for the different mines are shown in **Table 1** and **Figure 3**. It can be seen that the geothermal gradient is 1.12–5.56 °C/100 m, with an average of 3.32°C/100 m, inferring that the Pingdingshan coalfield is an area with an abnormally high ground temperature. It is interesting that the areas between the No. 13 mine and Shoushan No.1 mine show a high geothermal gradient.

The cap rock geothermal gradients are controlled by the buried depth of the Cambrian limestone reservoir. The results are shown in **Table 4**. In general, the geothermal gradient at buried depths less than 550 m is relatively low, with an average of 2.01°C/100 m. The geothermal gradient at buried depths of 600–850 m is relatively high, with an average of 3.96°C/100 m. The geothermal gradient at buried depths of more than 900 m is also low, with an average of 2.93°C/100 m.

TABLE 2 | Thermal conductivity of the Cambrian limestone (W/mK).

Coalfields	Locations	Sratum	Lithology	Thermal conductivity	Average
Pingding shan	Cambrian limestone exposed area	Zhangxia Formation in Cambrian system	Dolomite	3.050	3.837
	No. 11 mine			3.241	
	Shoushan No.1 mine			4.166	
	No. 2 mine			4.889	
	Xiangshan mine	Gushan Formation in Cambrian system	Dolomite limestone	1.501	2.420
	No. 11 mine			2.871	
	No. 9 mine			2.560	
	Shengli bridge			2.448	
	No. 13 mine			2.680	
	No. 5 mine			2.461	
	Average			2.987	
Ruzhou	Well 1 of Chaochuan mine	Zhangxia Formation in Cambrian system	Dolomite	3.036	

TABLE 3 | Measured contents of radionuclides in the different strata.

Times	Lithology	N_U (μg/g)	N_{Th} (μg/g)	N_K (%)	P (g/cm^3)
Quaternary	Clay	2.91	16.20	3.48	1.72
Neogene	Marl	2.18	11.60	1.51	1.47
Triassic Liujiagou formation	Sandstone	1.05	6.10	2.76	2.46
Permian Qianfeng formation	Sandstone	1.57	6.71	1.79	2.58
Upper Shihezi Formation of Permian	IV_2 coal	2.21	6.99	0.19	1.41
	V_2 coal	1.41	3.69	0.10	1.45
Lower Shihezi Formation of Permian	Mudstone	3.57	15.90	1.59	2.49
	Sandstone	1.80	8.68	1.72	2.63
Permian Shanxi Formation	Sandy mudstone	2.28	12.55	1.97	2.62
	II_1 coal	1.30	5.42	0.11	1.40
Carboniferous Taiyuan Formation	Sandstone	1.64	9.86	3.03	2.69
	Thin limestone	1.85	0.26	0.04	2.70
	Bauxite mudstone	2.93	16.40	4.46	2.65
	I_5 coal	1.99	3.65	0.09	1.32
Cambrian Gushan formation	Dolomitic limestone	2.96	5.12	3.06	2.68
Cambrian Zhangxia formation	Oolitic dolostone	2.77	1.36	0.29	2.75
Late Yanshanian magmatic rocks	Andesite	1.10	3.47	2.63	2.43
Mean Value		2.09	7.88	1.70	2.20

4.2 Calculating the Terrestrial Heat Flow

The Earth heat flux can be estimated by the Fourier formula:

$$q = 10 \times \lambda \times \theta \quad (1)$$

where q is the geothermal flow (mw/m^2), λ is the thermal conductivity of the surrounding rock (w/(mk)), and θ is the geothermal gradient (°C/100 m).

Based on the measured thermal conductivity of the limestone in the Cambrian system (**Table 2**), the average thermal conductivity of the oolitic dolomite of the Cambrian Zhangxia Formation in the Pingdingshan coalfield is 3.837 W/mK (**Table 5**), and that of the dolomitic limestone in the Gushan Formation is 2.420 W/m·K; the former is significantly higher than the latter. The average thermal conductivity of the Cambrian limestone throughout the whole coalfield is 2.987 W/m·K.

Because the areas near the southwest of the Guodishan Fault and northwest of the No. 13 mine are recharge areas of the Cambrian limestone, we may infer that the relatively low geothermal gradient is due to the influence of groundwater flow; so these areas were not used to calculate the ground heat flow. The calculations of the average geothermal gradient in different mines are shown in **Table 5**, where the heat flow value of each mine was obtained from **Eq. 1**. The mean values of the ground heat flow in the Pingdingshan coalfield is an abnormally high heat flow of 104.28 mW/m^2, which is much higher than the value of 65.88 mW/m^2 in the No. 1 well of the Chaochuan mine in the Ruzhou coalfield, 58.49 mW/m^2 in the Kaifeng Depression, and 62.63 mW/m^2 in the Tongxu Uplift.

4.3 Radiogenic Heat Generation in the Strata

4.3.1 The Computational Formula

The rock radiogenic heat generation rate refers to the heat generated in the decay process of radionuclides contained in rock per unit volume (or unit weight) per unit time. Uranium

TABLE 4 | Geothermal gradients at different burial depths (°C/100 m).

Buried depth the cambrian limestone reservoir (m)	Geothermal gradient	Buried depth the cambrian limestone reservoir (m)	Geothermal gradient	Buried depth the cambrian limestone reservoir (m)	Geothermal gradient
300 ± 25	1.79	600 ± 25	3.87	900 ± 25	3.08
350 ± 25	1.30	650 ± 25	3.75	950 ± 25	3.03
400 ± 25	1.97	700 ± 25	4.29	1,000 ± 25	2.60
450 ± 25	2.81	750 ± 25	4.33	1,050 ± 25	2.99
500 ± 25	3.05	800 ± 25	3.62	1,100 ± 25	3.28
550 ± 25	1.12	850 ± 25	3.91	1,150 ± 25	2.58
Average	2.01	Average	3.96	Average	2.93

TABLE 5 | Calculated heat flow in Pingdingshan and neighboring mining areas (mw/m^2).

Coalfield	Locations	Geothermal gradient (°C/100m)	Thermal conductivity (W/m·K)	Terrestrial heat flux	Average value
Pingding shan	Wuzhai mine	2.08	2.987	62.13	104.28
	No. 2 mine	2.69		80.35	
	No. 4 mines	3.10		92.60	
	No. 10 mines	3.12		93.19	
	No. 12 mines	3.34		99.77	
	No. 3 mines	3.73		111.42	
	No. 5 mines	3.85		115.00	
	No. 8 mines	4.06		121.27	
	No. 13 mines	4.27		127.54	
	Shoushan No.1 mine	4.67		139.49	
Ruzhou	Well 1 of Chaochuan mine	2.17	3.036	65.88	

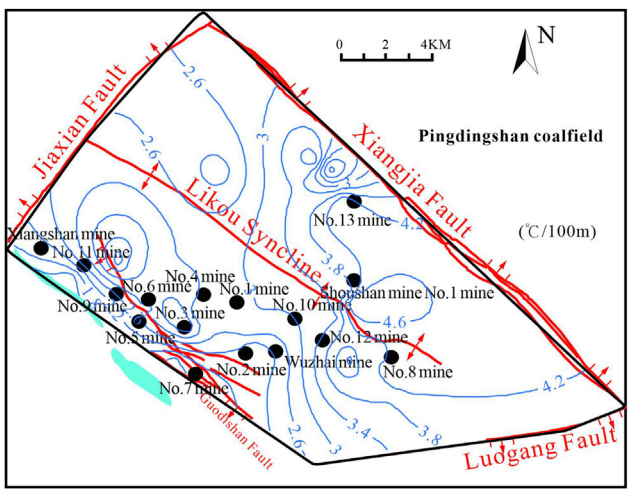

FIGURE 3 | Contour map of the geothermal gradient in the Pingdingshan coalfield.

($^{238}_{92}U$), thorium ($^{232}_{90}Th$), and potassium ($^{40}_{19}K$) in crustal rocks are three radionuclides that play an important role in the ground temperature because of their high abundances and high heat generation rates. Their half-lives (4.47×10^9 year, 1.40×10^{10} year, and 1.26×10^9 year, respectively) are equivalent to the Earth's age (4.55×10^9 year).

Based on the content of the radionuclides uranium, thorium, and potassium, and rock densities of the tested rock samples, the heat generation rate of radionuclides and the corresponding heat release can be calculated by using the Rybach formulas as:

$$Q_A = 0.01 \times \rho \times (9.52 \times N_U + 2.56 \times N_{Th} + 3.48 \times N_K) \quad (2)$$

$$Q = 0.001 \times \overline{Q_A} \times M \quad (3)$$

where Q_A is the heat generation rate of radionuclides in the rocks ($\mu W/m^3$), $\overline{Q_A}$ is the heat generation rate of radionuclides in the rock formation ($\mu W/m^3$), N_U is the U content in the rock ($\mu g/g$), N_{Th} is Th content in the rock ($\mu g/g$), N_K is the K content in the rock (%), $\boldsymbol{\rho}$ is the rock density (g/cm^3), Q is the radiogenic heat generation in the rock formation (mW/m^2), and M is the stratum depth (m).

4.3.2 Content of Radionuclides

According to the measured values of uranium, thorium, and potassium in the 40 rock samples collected from the Pingdingshan coalfield, their contents calculated as a function of time are shown in **Figures 4–6**, respectively. Obviously, the largest content of uranium, thorium, and potassium-40 in the Pingdingshan coalfield are, respectively, in the mudstone of the Lower Shihezi Formation, the bauxite mudstone of the carboniferous Taiyuan Formation, and the bauxite mudstone of the Carboniferous Permian Taiyuan Formation. The lowest contents are found in the sandstone of the Liujiagou Formation,

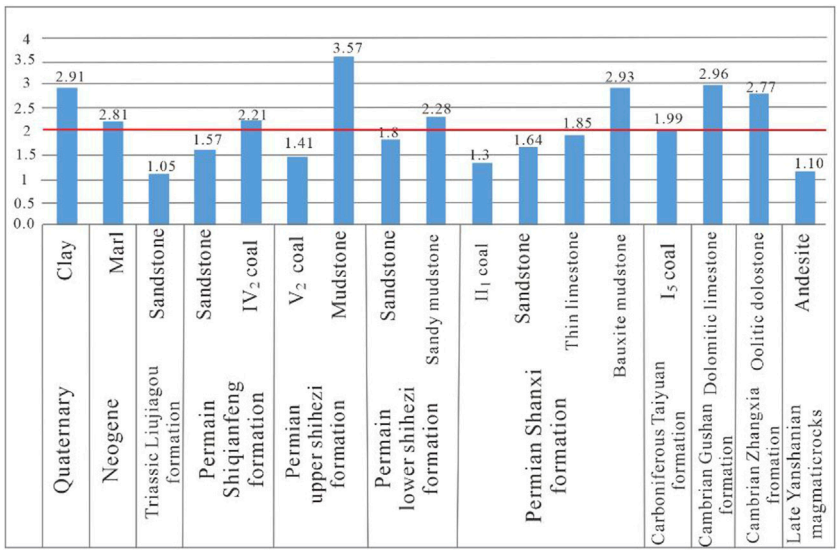

FIGURE 4 | Uranium content in the different strata (μg/g).

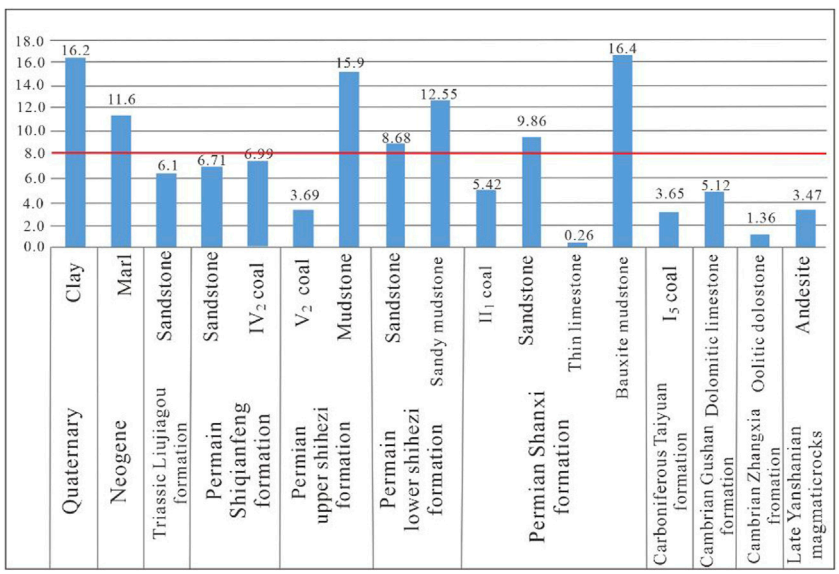

FIGURE 5 | Thorium content in the different strata (μg/g).

the limestone of the carboniferous Taiyuan Formation, and the limestone of carboniferous Triassic Taiyuan Formation, respectively. **Figures 4–6** show that the content of radionuclides in the magmatic rocks is at a relatively low level.

4.3.3 Radiogenic Heat Generation

The heat generation rate of radionuclides of different lithologies in the Pingdingshan coalfield (**Figure 7**) can be obtained using **Eq. 2**. The highest heat generation rate was found for the bauxite mudstone of the carboniferous Taiyuan Formation, followed by the mudstone of the Permian Lower Shihezi Formation, and the lowest heat generation rates were measured in 52 coal samples obtained from the Permian upper Shihezi Formation and 15 coal samples taken from the carboniferous Taiyuan Formation. The order of heat generation rate of the various lithology is mudstone > clay > thick limestone > sandstone > marl > andesite > thin limestone > coal seam; that is, the higher the argillaceous composition, the greater the heat generation rate.

The average radiogenic heat generation rate of the late Cambrian strata in the Pingdingshan coalfield is 1.05 $\mu W/m^3$, the thickness of which is about 800 m. The average heat generation rate of radionuclides in the Cambrian strata is

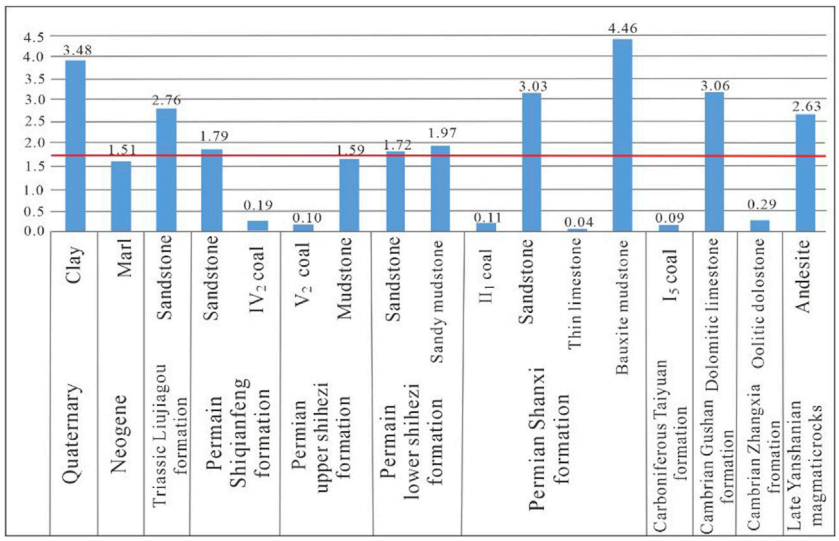

FIGURE 6 | Potassium-40 content in the different strata (%).

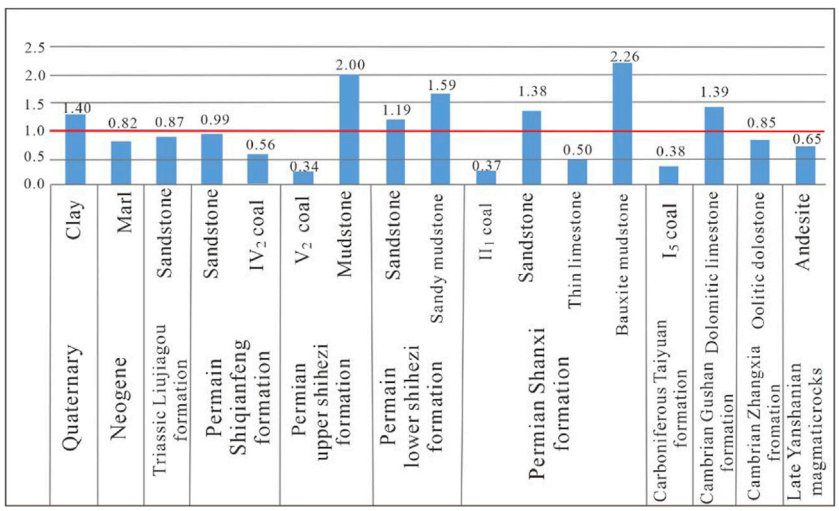

FIGURE 7 | Rate of radiogenic heat generation in the different strata (μW/m^3).

1.12 μW/m^3, whose thickness is about 300 m. The heat generation rate of radionuclides in the magmatic rock is 0.69 μW/m^3, for a thickness of 500 m. The radiogenic heat generation rates in the late Cambrian strata, Cambrian strata, and magmatic rocks in the coalfield are 0.84, 0.34, and 0.35 mW/m^2, respectively, where the sum of the three is 1.53 mW/m^2.

Overall, the contribution rate of the radiogenic heat generation in the sedimentary rocks and magmatic rocks in the Pingdingshan coalfield is only 1.47% of the local large geothermal flow value of 104.28 mW/m^2, which is at a very low level. Therefore, we may infer that the abnormally high ground temperature in the Pingdingshan coalfield is not caused by the radiogenic heat generation in the sedimentary strata or magmatic rocks.

4.4 Heat Release of Magmatic Rocks

4.4.1 Distribution of Magmatic Rocks

A magmatic rock intrusion was found during coal seam mining of the No. 13 coal mine in the Pingdingshan coalfield. The main lithology is neutral diorite porphyrite and basic diabase. The rock mass strikes northeast, with a length of 860 m and a maximum width of 60 m. A dyke intruded into the coal bearing strata, resulting in the existence of natural coke in the second group of coal seams.

TABLE 6 | Temperature of the ejected lava in the different volcanic areas (°C).

Types	Compositions	T	Locations	Source
Acidic	Rhyolite (lava, fused tuff, pumice flow)	735–780	Taupo, New Zealand	Ewart et al. (1971)
	Pyroxene rhyolite (pumice flow)	860–890	Taupo, New Zealand	Ewart et al. (1971)
	Rhyolitic dacite pumice	880	New Britain in the Western Pacific	Herming and Carmichael (1973)
	Rhyolitic dacite Obsidian	900–925	Iceland	Carmichael (1967)
Neutral	Dacite lava and pumice	925	New Britain in the Western Pacific	Herming and Carmichael (1973)
	Andesitic pumice	940–990	New Britain in the Western Pacific	Herming and Carmichael (1973)
Basic	leucite basalt	1,095	Muragira, Congo	Verhoogen (1948)
	Basaltic andesite	1,020–1,110	Parikuting, Mexico	Zies (1946)
	Tholeiitic basalt	1,150–1,225	Kilauea, Hawaii	Wright et al. (1968)

Magmatic rocks are exposed in the Dongshan area of the Dazhuang mine, Shilong District, Pingdingshan City, with an area of about 2 km^2 and a maximum thickness of 337.9 m, showing in **Figure 1**. The lithology mainly includes neutral andesite and andesite porphyrite. The magmatic rock mass in the coal-bearing strata is mainly shallow intrusive bedrock, dyke, and stock. From the perspective of the magma intrusion into different coal bearing sections and Neogene strata, the latest activity age should be the Neogene. Judging from the fact that the dyke was cut by the Yanshanian Liuzhuang Fault, the magmatism already formed in the Yanshanian Period.

In addition, a large area of magmatic rocks is exposed in the mountainous area of Lushan County, Pingdingshan City (**Figure 1**). The lithology is mainly late Yanshanian alkaline aegirine syenite, while acid granite porphyry and granite are also exposed locally. Shangtang, Zhongtang, Xiatang, and Jianchang hot springs are distributed along the Checun Fault that cuts through the magmatic rocks from top to bottom, and the temperatures of the springs are 71°C, 63°C, 64°C, and 35°C, respectively, indicating that there is also an abundant heat source in this zone.

4.4.2 Heat Generation of the Magmatic Rocks

The latest active age of the magmatic rocks exposed in the Dazhuang mine was during the Neogene, and its age is estimated to be about 35 Ma. In Mogou, southeast of Song County, Henan Province, which has the same age and lithology as Lushan's magmatic rocks, Mao et al. (2010) extracted intrusive alkaline rock samples of late Yanshan Cretaceous aegirine gabbro syenite and Indosinian syenite, and determined their ages to be 108 Ma and 194 Ma, respectively, using shrimp zircon. At the same site, Ren et al. (2001) and Lu et al. (2013) measured the ages of Indosinian syenites to be 208.5 ± 6.2 Ma and 245.5 ± 8.0 Ma, respectively (Fugen et al., 2001; Ren et al., 2013). In addition, Hou et al. (2007) measured the age of Late Mesozoic magmatic rocks from ^{40}Ar and ^{39}Ar isotopes in Dabie Mountain, finding 125–190 Ma (Hou et al., 2007). In conclusion, the activity of the intrusive neutral diorite porphyrite and basic diabase in the Pingdingshan coalfield began in the late Yanshanian Cretaceous and ended in the Himalayan Neogene, and has an age of 35–108 Ma.

The temperature of modern volcanic eruption lava measured directly on site shows that the magma composition is from acidic to basic, and the temperature of eruption lava was 735°C–1,225°C (**Table 6**) (Xu and Qiu, 2012). The intrusive magmatic rocks in the Pingdingshan coalfield are neutral diorite porphyrite and basic diabase. It is speculated that the lava temperature was more than 900°C.

At present, there have been a few literature studies on the cooling rate of neutral diorite porphyrite and basic diabase. Therefore, this paper compares the cooling rates of magmatic rocks in the Pingdingshan coalfield with the cooling rates of magmatic rocks with the same or similar lithology. Hourgian et al. (2004) found that the cooling rate of neutral syenite is 20°C/Ma in Kamchatka, Russia. For the basic cave granite in the late Yanshanian period in Zhangzhou, Fujian Province, studies by Shen et al. (2000) have shown, according to the isotope dating results and the closed temperature data in the different isotope systems, that igneous rocks always have changing cooling rates during the various geologic periods, such as, 103.0–97.1 Ma, 97.1–63.1 Ma, 63.1–57.5 Ma, 57.5–54.7 Ma corresponding to 16.9°C/Ma, 7.3°C/Ma, 8.9°C/Ma, and 53.6°C/Ma, respectively, with an average of 11.3°C/Ma. Therefore, it is estimated that the cooling rate of neutral diorite porphyrite and basic diabase in the Pingdingshan coalfield ranges from 11.3 to 20°C/Ma (Shen et al., 2000).

The latest intrusion time of the magmatic rock mass in the Pingdingshan coalfield is 35 Ma; with a lava temperature of 900°C. Therefore, assuming the cooling rate was 20°C/Ma, it is estimated that the residual temperature of the magmatic rock mass is more than 200°C. The higher residual temperature of the magmatic rock may cause its heat to be continuously transmitted upward through the rock strata or upward through faults, which provided a foundation for the high geothermal flow in the Pingdingshan coalfield. The conceptual model of abnormally high ground temperature caused by magmatic rocks is shown in **Figure 8**. Of course, the distribution of the ground temperature in the Pingdingshan coalfield seems to be uneven, which may be mainly controlled by the distributions of the different geological structures, intrusive rock mass distribution, Cambrian limestone groundwater migration, rock stratum structure, overburden performance, and other factors; however, further investigation of the effects of these structures and formations on the ground temperature distribution in the Pingdingshan coalfield is beyond the scope of the current study.

4.5 Discussion

In this study, we measured the outlet temperature values of 45 geothermal wells and water drains, and the thermal conductivity of 11 rock samples in the Cambrian layer. The measuring and sampling locations in the Cambrian layers with different burial depths are well-distributed, so the calculated geothermal gradient and

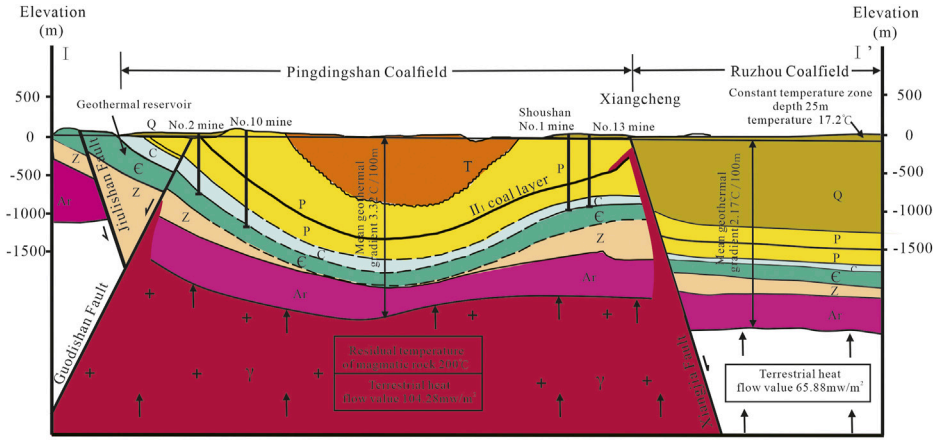

FIGURE 8 | Conceptual model diagram of geothermal genesis.

geothermal heat flow values can represent the true conditions in the abnormal Pingdingshan geothermal area. Based on the contents of the main radionuclides, the amounts of radiogenic heat production and their contributions for terrestrial heat flow were calculated quantificationally, and radiogenic heat production only has a 1.47% proportion of the whole terrestrial heat flow in the Pingdingshan area, which allows us to conclude that the influence of radiogenic heat generation on the abnormally high geothermal temperature in the Pingdingshan coal field can be excluded. In view of the intrusion of magmatic rocks in the 13 mines of the Pingdingshan coalfield and the neighboring area (Dazhuang Mine), it is can be inferred that the abnormally high ground temperature may likely be caused by the continuous heat release of magmatic rocks, and the conclusion that the residual temperature of the magmatic rock body is more than 200°C seems to be credible, agreeing with relevant research at similar conditions.

In the future, gravity prospecting and 3D seismic method can be further used to explore the characteristics of deep rock structure and fault distribution. A geothermal, geologic, hydrogeologic, and mathematical model will be constructed to ascertain the heat production and locate the high temperature target areas and layers in Pingdingshan. The geothermal wells (boreholes) will be constructed in the remained spaces after excavating coal, and the mathematical models can also be calibrated to predict the reservoir temperatures at different locations and depths accurately, providing technical support for the protecting the reservoirs in Pingdingshan coalfield and exploiting the deep geothermal energy.

5 CONCLUSION

Based on the discussions above, we can obtain the following conclusions:

1) The geothermal gradients of the Pingdingshan coalfield range from 1.12 to 5.56°C/100 m, with an average value of 3.32°C/100 m. The calculated values of heat flow in this coalfield is 62.13–139.49 mW/m^2, with an average value of 104.28 mW/m^2. Therefore, we can conclude that the Pingdingshan coalfield belongs to an abnormal geothermal area.
2) The radiogenic heat generation rates of the late Cambrian strata, Cambrian strata, and magmatic rocks in the coalfield are 0.84 mW/m^2, 0.34 mW/m^2, and 0.35 mW/m^2, respectively, with a sum of 1.53 mW/m^2. The contribution rate of the radiogenic heat generation to the local large geothermal flow value is only 1.47%, which is at a very low level.
3) Neutral diorite porphyrite and a basic diabase intrusion were found during mining in the No. 13 coal mine, while neutral andesite and andesite porphyrite were exposed in the Dazhuang coal mine near the Pingdingshan coalfield. The heat release of magmatic rock may be the primary heat source causing the abnormally high ground temperature in Pingdingshan.
4) In the Pingdingshan area, the intrusion time of the magmatic rock mass is about 35 Ma and the lava temperature is about 900°C. Assuming the cooling rate is 20°C/Ma, we can obtain the residual temperature of the magmatic rock mass, which is more than 200°C. The relatively high residual temperature of the magmatic rock may be the main heat source of the abnormally high ground temperature in this coalfield.

DATA AVAILABILITY STATEMENT

The original contributions presented in the study are included in the article/Supplementary Material, further inquiries can be directed to the corresponding author.

AUTHOR CONTRIBUTIONS

All authors listed have made a substantial, direct, and intellectual contribution to the work and approved it for publication.

FUNDING

This work was supported by the National Natural Science Foundation of China (41802186, 41972254), the Innovation

Scientists and Technicians Troop Construction Projects of Henan Province (Grant CXTD2016053), and the Fundamental Research Funds for the Henan Polytechnic University (NSFRF200103).

REFERENCES

Bingqi, C., Xinyi, W., and Jiale, Z. (2014). Analysis on Temperature Distribution and Influencing Facators in Pingdingshan Coal Field. *Coal Technol.* 33 (07), 73–75. doi:10.2514/6.2008-2309

Burns, E. R., Williams, C. F., Ingebritsen, S. E., Voss, C. I., Spane, F. A., and DeAngelo, J. (2015). Understanding Heat and Groundwater Flow through Continental Flood Basalt Provinces: Insights Gained from Alternative Models of Permeability/depth Relationships for the Columbia Plateau, USA. *Geofuilds* 15, 120–138. doi:10.1002/9781119166573.ch13

Erbek, E., and Dolmaz, M. N. (2019). Investigation of the Thermal Structure and Radiogenic Heat Production through Aeromagnetic Data for the Southeastern Aegean Sea and Western Part of Turkey. *Geothermics* 81, 113–122. doi:10.1016/j.geothermics.2019.04.011

Fugen, R., Yanjie, Y., Shuangbao, L., and Jianong, Z. (2001). The Coupling Character between Isotopic Geochronology of Indosinian Epoch in Xiong'er Fault Basin. *Bull. Mineralogy, Petrology Geochem.* 2001 (04), 286–288. doi:10.3969/j.issn.1007-2802.2001.04.022

Hasterok, D., Gard, M., and Webb, J. (2018). On the Radiogenic Heat Production of Metamorphic, Igneous, and Sedimentary Rocks. *Geosci. Front.* 9 (6), 1777–1794. doi:10.1016/j.gsf.2017.10.012

Hou, Q., Liu, Q., Li, J., Zhang, H., and Zhang, X. (2007). Late Mesozoic Shear Zones and its Chronology in the Dab Ie Mountains, Central China. *Chin. J. Geol. Sci. Geol. Sinica)* 2007 (01), 114–123. doi:10.1155/2012/291467

Hourgian, J. K., Soloviev, A. V., and Ledneva, G. V. (2004). Timing of Syenite Intrusions on the Eastern Slope of Sredinnyi Range, Kamchatka: Rate of Accretionary Structure Exhumation. *Geochem. Int.* 42 (2), 131–141. doi:10.1144/1467-7873/03-024

Jun, P., Wen, W. J., and Tao, P. (2015). Distribution Characteristics and Abnormal Factors of Geothermal Field in Linhuan Mine Area. *Coal Eng.* 47 (01), 88–91. doi:10.11799/ce201501028

Lu-sheng, S., Qiu-xiang, H., and Shan-shan, C. (2020). Characteristics of Radioactive Heat Generatio Rate of Granites in the Southeastern Jiangxi Province. *J. East China Univ. Technol. Sci.* 43 (06), 514–520. doi:10.3969/j.issn.1674-3504.2020.06.002

Luo, X., Zhu, C., Zhang, B., Boning, T., and Tiange, C. (2020). Heat Production Rate Calculation Using Gamma-Raylogging of the Sedimentary for Mation in the Tarimbasin,Northwest China. *Acta Geol. Sin.* 94 (07), 2078–2088. doi:10.19762/j.cnki.dizhixuebao.2020219

Mao, J.-W., Xie, G.-Q., Pirajno, F., Ye, H.-S., Wang, Y.-B., Li, Y.-F., et al. (2010). Late Jurassic-Early Cretaceous Granitoid Magmatism in Eastern Qinling, Central-Eastern China: SHRIMP Zircon U-Pb Ages and Tectonic Implications. *Aust. J. Earth Sci.* 57, 51–78. doi:10.1080/08120090903416203

Ogunsanwo, F. O., Adepitan, J. O., Ayanda, J. D., Giwa, K. W., Falayi, E. O., and Adejimi, A. I. (2021). Radiogenic Heat Production in Crustal Quarry Rocks of Ogun State, South-Western, Nigeria. *Environ. Earth Sci.* 80 (7), 1–15. doi:10.1007/s12665-021-09578-7

Ren, L., Tao, L., Fengjun, B., and Xinxiang, L. (2013). LA-ICP-MS U-Pb Zircon Age and Hf Isotope Composition of Mogou Syenite, Western Henan Province. *Geol. Rev.* 59 (02), 355–368. doi:10.3969/j.issn.0371-5736.2013.02.017

Ren, Z., Wu, J., and Peng, T. (2017). Radiogenic Heat Production of Magmatic Rock of Coal Measure Strata Based on Natural Gamma-Ray Logging in Zhuji Mine Field of Huainan Coal Field. *Coal Geol. Explor.* 45 (03), 49–53+58. doi:10.3969/j.issn.1001-1986.2017.03.009

Scharfenberg, L., Regelous, A., and De Wall, H. (2019). Radiogenic Heat Production of Variscan Granites from the Western Bohemian Massif, Germany. *J. Geosciences* 64 (4), 251–269. doi:10.3190/jgeosci.293

Shen, W., Ling, H., Li, H., Li, W., Wang, D, et al. (2000). Thermal Evolution History of Xincun Cave Granite in Fujian Province. *Chin. Sci. Bull.* 2000 (14), 1538–1543. doi:10.3321/j.issn:0023-074X.2000.14.016

Sun, M., Liu, D., Kang, Z., Guan, Y., Liang, G., Huang, X., et al. (2020). Analysis of Hot-Dry Geothermal Resource Potential in Southeastern Guangxi. *Earth Sci. Front.* 27 (01), 72–80. doi:10.13745/j.esf.2020.1.9

Veikkolainen, T., and Kukkonen, I. T. (2019). Highly Varying Radiogenic Heat Production in Finland, Fennoscandian Shield. *Tectonophysics* 750, 93–116. doi:10.1016/j.tecto.2018.11.006

Veikkolainen, T., Kukkonen, I. T., and Näslund, J.-O. (2019). Radiogenic Heat Production Analysis of Fennoscandian Shield and Adjacent Areas in Sweden. *Geophys. J. Int.* 218 (1), 640–654. doi:10.1093/gji/ggz186

Wang, Z., Jiang, G., Zhang, C., Hu, J., Shi, Y., Wang, Y., et al. (2019). Thermal Regime of the Lithosphere and Geothermal Potential in Xiong'an New Area. *Energy Explor. Exploitation* 37 (2), 787–810. doi:10.1177/0144598718778163

Weinert, S., Bär, K., Scheuvens, D., and Sass, I. (2021). Radiogenic Heat Production of Crystalline Rocks in the Gonghe Basin Complex (Northeastern Qinghai–Tibet Plateau, China). *Environ. Earth Sci.* 80 (7), 1–19. doi:10.1007/s12665-021-09558-x

Xin, M. A., Lei, F., and Tiefeng, L. I. (2021). Analysis of Geothermal Origin in Eastern Himalayan Syntaxis. *Geoscience* 35 (01), 209–219. doi:10.19657/j.geoscience.1000-8527.2021.016

Xu, X., and Qiu, J. (2012). *Igneous Petrology*. Beijing: Science Press.

Zhang, C., Hu, S., Song, R., et al. (2020). Genesis of the Hot Dry Rock Geothermal Resources in the Gonghe Basin: Constraints from the Radiogenic Heat Production Rate of Rocks. *Chin. J. Geophys.* 63 (7), 2697–2709. doi:10.6038/cjg2020N0381

Zhang, C., Hu, S., Zhang, S., Li, S., Zhang, L., Kong, Y., et al. (2020). Radiogenic Heat Production Variations in the Gonghe Basin, Northeastern Tibetan Plateau: Implications for the Origin of High-Temperature Geothermal Resources. *Renew. Energy* 148, 284–297. doi:10.1016/j.renene.2019.11.156

Zhang, F., Wang, G., and Hou, X. (2000). An Analysis of the Formation of Geothermal Resources and the Effects of Groundwater Circulation on the Wall Rock Temperature Field –Taking the Pingdingshan Mining Field as an Example. *Acta Geosci. Sin.* 2, 142–146. doi:10.3321/j.issn:1006-3021

Zhao, X., Zeng, Z., Huai, N., and Wang, K. (2020). Geophysical Responses and Possible Geothermal Mechanism in the Gonghe Basin, China. *Geomechanics Geophys. Geo-Energy Geo-Resources* 6 (1), 1–12. doi:10.1007/s40948-020-00141-5

Conflict of Interest: The authors declare that the research was conducted in the absence of any commercial or financial relationships that could be construed as a potential conflict of interest.

Publisher's Note: All claims expressed in this article are solely those of the authors and do not necessarily represent those of their affiliated organizations, or those of the publisher, the editors and the reviewers. Any product that may be evaluated in this article, or claim that may be made by its manufacturer, is not guaranteed or endorsed by the publisher.